JCTC Journal of Chemical Theory and Computation

Article

pubs.acs.org/JCTC

Electronic Excitation Energies in Dimers between Radical Ions Presenting Long, Multicenter Bonding

Maria Fumanal, Marçal Capdevila-Cortada,*,† Jordi Ribas-Arino, and Juan J. Novoa

Departament de Química Física and IQTCUB, Facultat de Química, Universitat de Barcelona, Avenida Diagonal 645, 08028 Barcelona, Spain

Supporting Information

ABSTRACT: The formation of long, multicenter dimers between radical ions is usually monitored through UV−vis spectroscopy given the characteristic low-energy absorption band that they exhibit, not observed for the parent monomers. In this work, the performance of CASPT2, RASPT2, and TD-DFT methods for obtaining excitation energies of the long, multicenter bonded π-$[TCNE]_2^{2-}$ and π-$[TTF]_2^{2+}$ dimers has been addressed (TCNE = tetracyanoethylene; TTF = tetrathiafulvalene). The impact of the active space on the vertical electronic transitions computed at the RASPT2 and CASPT2 levels has been tested against experimentally observed absorption bands. Analogous tests have been carried out for a wide variety of density functionals within the TD-DFT formalism. Our calculations show that whereas CASPT2 predicts very accurate excitation energies for the π-$[TCNE]_2^{2-}$, the mean absolute error for π-$[TTF]_2^{2+}$ is higher for CASPT2 than for TD-DFT calculations, whenever pure density functionals or low % HF exchange hybrid functionals are used. Hybrid functionals with high % HF exchange (and thus RSH functionals) conduct to large errors on the excitation energies in both dimers. Furthermore, vertical electronic transitions are also obtained for 100 configurations extracted from a 45 ps molecular dynamics (CPMD) simulation aimed at providing an accurate description of the thermal fluctuation effects of a π-$[TCNE]_2^{2-}$ dimer in dichloromethane. These thermal effects explain the shape of the experimental UV−vis spectrum, where the lowest HOMO → LUMO absorption presents a broad band and the following HOMO-1 → LUMO absorption exhibits a narrower band.

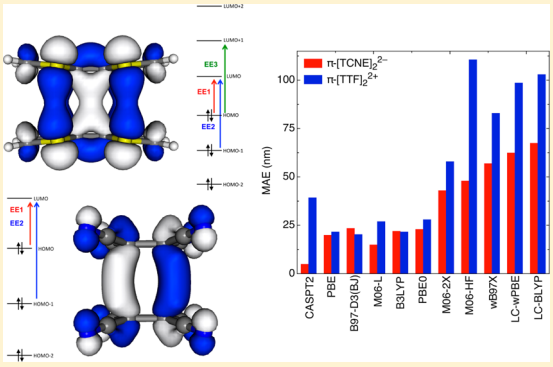

INTRODUCTION

Organic compounds with large electron donor or acceptor capability are of general interest due to their application in conducting,[1] superconducting,[2] or magnetic materials.[3−5] It is well established that these compounds, once oxidized (donors) or reduced (acceptors), become radical ions that can dimerize leading to diamagnetic entities,[6−8] and this process ultimately has severe implications on the aforementioned properties. The bonding nature behind these dimers differs from conventional covalent bonds in two major points:[8−10] (1) isolated dimers of radical ions are metastable (i.e., despite being unstable toward dissociation, they are bound due to an associated energy barrier of around 5 kcal mol^{-1}), and (2) their equilibrium distance is much longer than covalent bonds (around 2.9 Å in π-$[TCNE]_2^{2-}$, for instance), although still shorter than van der Waals interactions (typically around 3.4 Å for two neutral TCNE interacting molecules). The metastable character arises from the stabilization obtained by the bonding term (as a result of the double occupation of the SOMOs bonding combination) plus the dispersion term, although it is not large enough to defeat the Coulombic repulsion between the radical ions.[11] However, they do form in the solid state and in low-temperature solutions due to the interactions between the long-bonded dimer and the adjacent counterions or solvent molecules, respectively, which overcome the repulsion between the radical ions that form the dimer.[9,12,13] Long, multicenter (sometimes also referred as pancake) bonding has largely been characterized by several spectroscopic techniques, such as UV−vis,[7,14−16] EPR,[17−20] IR,[7,16] or Raman[21] spectroscopies, and it has been observed in dimers of radical anions such as tetracyanoethylene (TCNE, Scheme 1),[6,7] radical cations such as tetrathiafulvalene (TTF, Scheme 1),[13] neutral radicals such as phenalenyl derivatives,[17,22,23] and the zwitterionic charge-transfer dyad π-$[TTF^{\partial+}\cdots TCNE^{\partial-}]$.[24] Moreover, several supramolecular entities involving long, multicenter bonding have

Scheme 1. Chemical Structures of Tetracyanoethylene (TCNE) andTtetrathiafulvalene (TTF) Molecules

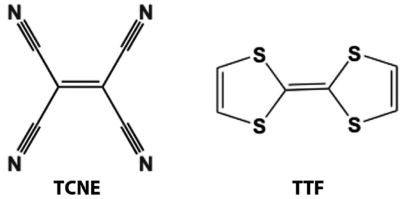

TCNE TTF

Received: April 23, 2015

DOI: 10.1021/acs.jctc.5b00381
J. Chem. Theory Comput. XXXX, XXX, XXX−XXX

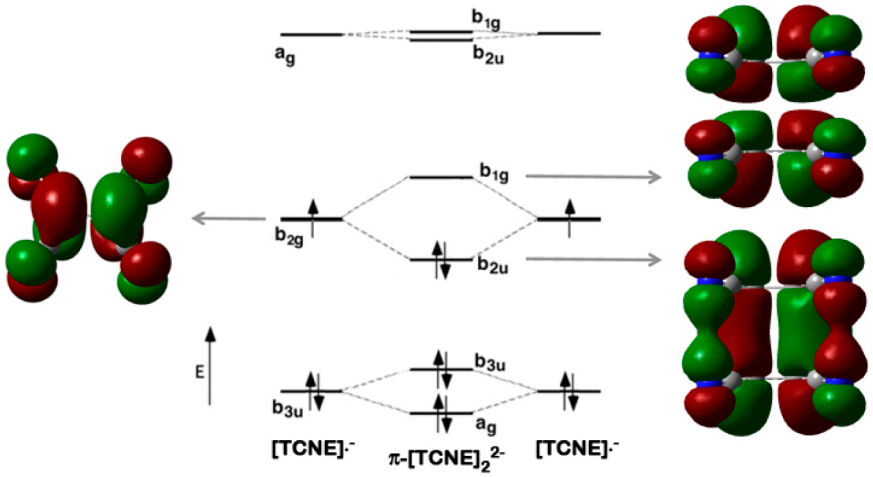

Figure 1. Molecular orbital diagram (limited to the frontier region) of the π-$[TCNE]_2^{2-}$ dimer. $[TCNE]^{\bullet-}$ SOMO orbital (left) and π-$[TCNE]_2^{2-}$ HOMO and LUMO orbitals (right) are also depicted.

lately been reported[20,25−27] and computationally evaluated.[28−30] These aggregates have been recently suggested as promising candidates for their potential application in molecular recognition processes and molecular switches.[31]

Among the aforementioned spectroscopic techniques, UV−vis spectroscopy is the most common to probe the presence of long, multicenter bonded dimers. Organic radical ions, upon dimerization, typically show a characteristic broad band at higher wavelength than the lowest energy electronic transition band of the parent radical ion.[14,15] On the resulting dimer, all orbitals of the parent monomers combine and constitute the orbitals of the dimer. In particular, the new characteristic band is a result of the overlap between the SOMOs of each radical ion, which combine and form a bonding and an antibonding combinations, the former being doubly occupied whereas the latter being empty.[8] The higher this overlap is, the more energetic the HOMO → LUMO transition will be. All this is exemplified for the π-$[TCNE]_2^{2-}$ dimer in Figure 1, although this is also the case of π-$[TCNQ]_2^{2-}$, π-$[TCNP]_2^{2-}$, π-$[TTF]_2^{2+}$, or π-$[OMB]_2^{2+}$ dimers, to mention just a few examples. Kochi et al. thoroughly studied the dimerization of several organic radicals in solution,[14,15,17] where they determined the equilibrium constants, K_D, and enthalpies and entropies of dimerization (ΔH_D and ΔS_D) by means of UV−vis and EPR measurements as a function of the temperature.

Multiple attempts have been done to predict and probe the formation of such dimers making use of their UV−vis spectrum as a baseline, usually carried out by means of TD-DFT calculations.[32−36] However, to date there are no studies neither evaluating or comparing density functionals or other methods for the analysis of electronic excitations on these specific dimers nor providing clues concerning the appropriateness of the computational setup. The present work focuses on CASPT2 and TD-DFT calculations of vertical electronic transitions aiming at establishing a reliable benchmarked computational method (among the common ones) to successfully assess electronic excitation energies of dimers presenting long, multicenter bonding. These calculations were done on DFT optimized geometries for the π-$[TCNE]_2^{2-}$ and the π-$[TTF]_2^{2+}$ dimers, as well as on 100 configurations obtained from a 45 ps molecular dynamics simulation reproducing the solution environment of a π-$[TCNE]_2^{2-}$ dimer on dichloromethane. The latter approach permits the evaluation of the effects of thermal fluctuations on the UV−vis spectrum of a given system and has already been shown to provide important insights on the study of several physical properties.[37−46]

METHODOLOGY

Vertical electronic transitions were obtained by means of CASPT2 (RASPT2) and TD-DFT calculations. Several active spaces for the CASPT2 (RASPT2) calculations were considered on both π-$[TCNE]_2^{2-}$ and π-$[TTF]_2^{2+}$ dimers. The CASSCF (RASSCF) reference wave functions were obtained using the state-averaged (SA) method. In a recent work we showed that although the wave function of these two dimers is already well described with a minimal (2,2) active space, the direct π-space is required to achieve quantitative interaction energies.[47] For the present study, the CAS(2,2), CAS(4,3), CAS(6,4), and RAS(22,2,2;8,4,8) active spaces were used on the π-$[TCNE]_2^{2-}$, whereas the CAS(2,2), CAS(2,4), CAS(4,4), CAS(6,4), CAS(6,6), and RAS(26,2,2;10,6,4) were considered on the π-$[TTF]_2^{2+}$ dimer. For both dimers, the RAS spaces comprise the direct π-space, i.e., a (22,20) for the former dimer and a (26,20) for the latter, with different RAS2 subspaces (namely, (6,4) for π-$[TCNE]_2^{2-}$ and (6,6) for π-$[TTF]_2^{2+}$).

The TD-DFT calculations were carried out using 10 density functionals, including generalized gradient approximation (GGA), meta-GGA, hybrid GGA, hybrid meta-GGA, and range-separated hybrid (RSH) functionals. The density functionals considered in this work are the pure GGA functionals PBE[48] and B97-D3(BJ),[49] the meta-GGA M06-L,[50] the hybrid GGA functionals B3LYP[51,52] and PBE0 (which contain 20% and 25% of HF exchange, respectively), the M06-2X[53] (54% HF exchange) and M06-HF[54] hybrid meta-GGA (100% HF exchange), and the RSH functionals ωB97X,[55] LC-ωPBE,[56] and LC-BLYP.[52,57,58]

Various basis sets were used for this study. For both methodologies, CASPT2 (RASPT2) and TD-DFT, the basis set effects were evaluated as a preliminary step. The ANO-L basis sets,[59,60] contracted to DZP, TZP, and QZP, were used for the former methodology, whereas the 6-31+G(d), 6-311G, 6-311G(d), 6-311+G(d), and 6-311+G(2d) series,[61] TZVP,[62] def2-TZVP,[63] and aug-cc-pVTZ[64] basis sets were considered for the TD-DFT calculations. After the proper discussion comparing the results obtained with these basis sets (see next

DOI: 10.1021/acs.jctc.5b00381
J. Chem. Theory Comput. XXXX, XXX, XXX−XXX

section), the benchmark calculations were ultimately carried out using the TZP contraction of the ANO-L basis set for the CASPT2 (RASPT2) calculations and the 6-311+G(d) for the TD-DFT calculations.

The Results and Discussion section of this work is divided into two parts. For the first part, the static perspective, all excitation energies were obtained on previously optimized geometries at the PBE-D2/6-31+G(d) level in a solution environment modeled by means of the polarizable continuum model (PCM).[65,66] TD-DFT calculations on optimum geometries obtained using three other functionals (B97-D3(BJ), PBE-D3(BJ), and M06-L, the density functionals shown in ref 47 that best reproduced the equilibrium distances obtained at the RASPT2 level) revealed that the functional used to perform the geometry optimization has a minor impact on the vertical excitation energies (Supporting Information (SI) Table S1). Similarly, a set of calculations on the π-$[TCNE]_2^{2-}$ dimer combining explicit (via a $(CH_2Cl_2)_4$ cluster embedding the dimer) and implicit (via PCM) solution models showed that there is almost no improvement when the small cluster of explicit solvent molecules is added to the implicit modeling (SI Table S2). Therefore, the solution environment was modeled in all calculations using the PCM solvation model.

On the second part of this work, the effects of the thermal motion on the electronic transition energies were evaluated. For this study, 100 configurations equally distributed over the time were extracted from a 45 ps molecular dynamics simulation (*ab initio* molecular dynamics, AIMD) of the π-$[TCNE]_2^{2-}$ dimer in a dichloromethane simulation box, modeling the condensed phase and hence the solution environment. On each configuration, only π-$[TCNE]_2^{2-}$ was extracted from the simulation box, and solvent effects were added through the aforementioned continuum approach for the excitation energies calculations. The AIMD simulations were performed using the Car−Parrinello (CP) scheme for propagating the wave functions and the nuclear configurations as implemented in the CPMD package.[67] The PBE-D2 density functional[68] was used for the electronic structure calculations, together with Vanderbilt pseudopotentials,[69] and a wave function cutoff of 25 Ry. The time step was set to 4 au, and the fictitious mass for the orbitals was chosen to be 400 amu. A cubic simulation box (a = 18.331 Å) with periodic boundary conditions was used, which contained 64 CH_2Cl_2 molecules and one π-$[TCNE]_2^{2-}$ dimer. The initial configurations were taken from an equilibrated force-field MD simulation, which was followed by a further equilibration of 2 ps in the canonical ensemble, in order to let the system relax in the new (*ab initio*) interaction potential. The Nosé−Hoover thermostat[70−72] was used to get an average temperature of 175 K. The detailed structural analysis of the simulations will be discussed in a forthcoming report.

The standard IPEA Hamiltonian and the Cholesky decomposition of two-electron integrals were used for all multireference calculations.[73−75] All DFT optimizations and TD-DFT calculations were carried out using the Gaussian09 package,[76] whereas Molcas7.6 was used for CASSCF/CASPT2 and RASSCF/RASPT2 calculations.[77]

RESULTS AND DISCUSSION

A. Static Perspective. *A.1. CASPT2 (RASPT2) Vertical Electronic Transitions.* The UV−vis spectra of the π-$[TCNE]_2^{2-}$ and π-$[TTF]_2^{2+}$ dimers are first assessed in this section by means of CASPT2 (or RASPT2, when specified) calculations. These calculations are performed on previously optimized DFT geometries (see Methodology). The experimental UV−vis spectrum of the π-$[TCNE]_2^{2-}$ dimer presents two absorption bands at 525 and 370 nm in CH_2Cl_2, whereas the spectrum of the π-$[TTF]_2^{2+}$ dimer exhibits three bands at 730, 520, and 395 nm in acetone.[14,15]

The lowest vertical excitation energy is obtained for the π-$[TCNE]_2^{2-}$ dimer with the DZP, TZP, and QZP contractions of the ANO-L basis set, for several active spaces. The results are collected in Table 1 and evidence the impact of the basis set

Table 1. Lowest Electronic Excitation Energy Obtained at the CASPT2 and RASPT2 levels for the π-$[TCNE]_2^{2-}$ and π-$[TTF]_2^{2+}$ Dimers in the Gas Phase, for Different Active Spaces and ANO-L Basis Set Contractions[a]

	DZP	TZP	QZP
	π-$[TCNE]_2^{2-}$		
CAS(2,2)	467	479	481
CAS(4,3)	478	490	492
CAS(6,4)	480	491 (516)	492
RAS(22,20)	488	504	501
	π-$[TTF]_2^{2+}$		
CAS(2,2)		602	
CAS(2,4)		629	
CAS(4,4)		612	
CAS(6,4)		619	
CAS(6,6)		641 (663)	
RAS(26,20)		627	

[a]Values are given in nanometer units. Also given, in parentheses, are the results obtained using the PCM solvation model (dichloromethane and acetone, respectively).

effects on this first vertical electronic transition. For all active spaces the vertical excitation energies reach a convergence at the TZP contraction. It thus follows that the TZP contraction is of sufficient quality for obtaining accurate excitation energy values, and therefore it was applied for all next calculations.

The main issue of any multiconfigurational self-consistent field calculation is the choice of the active space. For the specific case of long-bonded π-dimers, the CAS(2,2) active space, which results from the bonding and antibonding combinations of the SOMO orbital of each parent radical monomer, allows one to calculate the first energy band, which arises from the HOMO → LUMO (H → L) electronic excitation in both π-$[TCNE]_2^{2-}$ and π-$[TTF]_2^{2+}$ dimers. However, the minimal active space is usually not accurate enough to obtain quantitative excitation energies, and larger active spaces are required. Furthermore, when not only the H → L but also higher energy transitions are evaluated, all orbitals involved in these electronic excitations must be included in the active space.

The two bands observed in the experimental UV−vis spectrum of π-$[TCNE]_2^{2-}$ correspond to the H → L and H-1 → L electronic transitions. Therefore, the minimum active space comprising the orbitals involved in these transitions is a CAS(4,3). Such an active space is formed by the bonding and antibonding combinations of the SOMOs of each parent $[TCNE]^{\bullet-}$ plus the antibonding combination of the doubly occupied orbital lying below its SOMO (see Figure 2). CAS(4,3) can thus be extended by adding the bonding combination of the latter orbitals, resulting in a CAS(6,4) active space, which was shown to provide an accurate

DOI: 10.1021/acs.jctc.5b00381
J. Chem. Theory Comput. XXXX, XXX, XXX−XXX

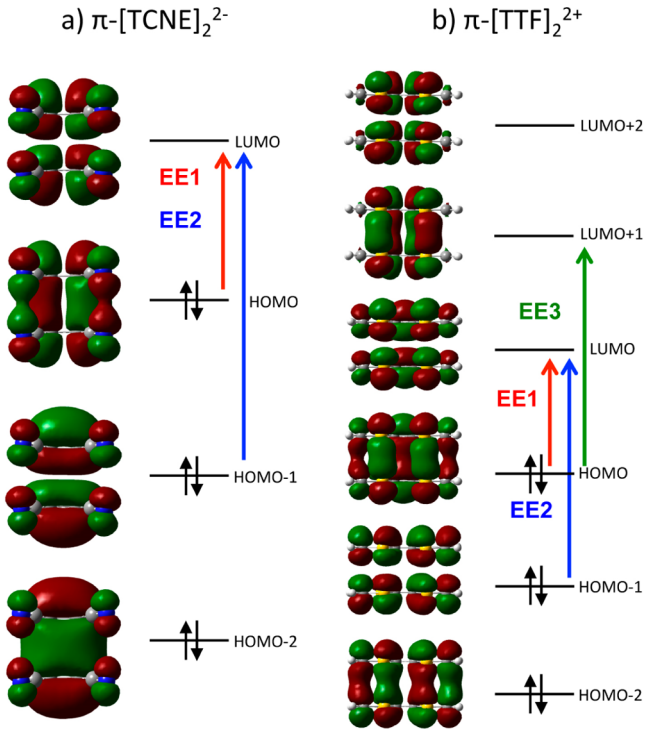

Figure 2. Molecular orbitals included in the (6,4) and (6,6) active spaces used for the (a) π-$[TCNE]_2^{2-}$ and (b) π-$[TTF]_2^{2+}$ excitation energies calculations. The vertical electronic transitions corresponding to the experimentally observed bands are depicted in both cases.

description of the wave function at geometries close to the equilibrium distance.[47] In addition to the aforementioned active spaces, the RAS(22,2,2;8,4,8) restricted active space has also been considered, in order to take into account the whole π-space in the active space (from now on, RAS(22,20); further details are given in Methodology). The (2,2), (4,3), and (6,4) active spaces of π-$[TCNE]_2^{2-}$ are shown in Figure 2a (the more extended RAS active space is given in SI Figure S1). Note the delocalized nature of all molecular orbitals. The lowest electronic excitation energy obtained at the CASPT2 or RASPT2 level using the aforementioned active spaces is given in Table 1. Although there is a clear improvement from CAS(4,3) and CAS(6,4) compared to the minimum CAS(2,2) results, convergence is not achieved until all π-orbitals are considered in the reference wave function. This result is consistent with the delocalized character of the orbitals. The excitation energy obtained with the larger RAS(22,20) active space (504 nm) is in good agreement with the experimental value (525 nm).

Similarly, the lowest excitation energy was also obtained for the π-$[TTF]_2^{2+}$ dimer with several active spaces. In addition to the minimal CAS(2,2) active space, CAS(2,4), CAS(4,4), CAS(6,4), and CAS(6,6) have also been considered, as well as the RAS(26,2,2;10,6,4) restricted active space (from now on, RAS(26,20)). In contrast to the π-$[TCNE]_2^{2-}$ dimer, in the π-$[TTF]_2^{2+}$ dication dimer each TTF was oxidized prior the dimerization process (instead of reduced, as in the former dimer), and thus the CAS(2,4) is the resulting active space analogous to the CAS(6,4) of the dianion dimer. Furthermore, the three bands observed in the experimental UV−vis spectrum correspond to the H → L, H-1 → L, and H → L+1 transitions, and thus CAS(4,4) is the minimum active space including these orbitals. The (2,2), (2,4), (4,4), (6,4), and (6,6) active spaces are shown in Figure 2b (the more extended RAS is shown in SI Figure S2). The lowest excitation energy, which corresponds to the H → L transition, is given in Table 1 at the CASPT2 (RASPT2) level using the aforementioned active spaces. The minimal CAS(2,2) underestimates the excitation energy (602 nm), whereas CAS(6,6) provides an energy larger than RAS (641 and 627 nm, respectively) but closer to the experimental value (730 nm). Similarly to the scenario found for π-$[TCNE]_2^{2-}$, the molecular orbitals of the π-$[TTF]_2^{2+}$ dimer are highly delocalized over the whole π-system, and thus the wave function at the CAS(2,2) level is barely well described.

The effects driven by the solution environment were investigated by means of PCM modeling considering dichloromethane and acetone solvents for π-$[TCNE]_2^{2-}$ and π-$[TTF]_2^{2+}$, respectively. The lowest excitation energy was obtained for the π-$[TCNE]_2^{2-}$ dimer with the CAS(6,4) active space and with the CAS(6,6) for the π-$[TTF]_2^{2+}$ dimer (values in parentheses of Table 1). For both cases, solvent effects lead to a shift on the excitation energies of ∼5% to lower values, obtaining excitation energies of 516 and 663 nm for the π-$[TCNE]_2^{2-}$ and π-$[TTF]_2^{2+}$ dimers, respectively. Thus, for both dimers the lowest excitation energy obtained in solution is closer to the experimental value (525 nm for π-$[TCNE]_2^{2-}$ and 730 nm for π-$[TTF]_2^{2+}$) than the gas phase result. These results reveal the small but not negligible impact of the solvent on the excitation energies induced by the presence of the polar environment.

The UV−vis spectra of both dimers have been finally computed at the CASPT2 level. In light of the previous results, the CAS(6,4) and CAS(6,6) active spaces were used for π-$[TCNE]_2^{2-}$ and π-$[TTF]_2^{2+}$, respectively, obtained in the PCM solvation model with the TZP contraction of the ANO-L basis set. Five CAS(6,4) singlet states were calculated for the π-$[TCNE]_2^{2-}$, whereas seven CAS(6,6) singlet roots were needed for the π-$[TTF]_2^{2+}$ dimer to account for the three allowed transitions observed in the experimental spectrum. The results obtained for both π-dimers are shown in Table 2 (non-

Table 2. CASPT2 Electronic Spectrum for the π-$[TCNE]_2^{2-}$ and π-$[TTF]_2^{2+}$ Dimers Obtained with the PCM Solution Model (Dichloromethane and Acetone, Respectively)[a]

	calc	expt
	π-$[TCNE]_2^{2-}$	
H → L	516 (0.3)	525 (1.6)
H-1 → L	368 (0.6)	370 (1.0)
	π-$[TTF]_2^{2+}$	
H → L	663 (0.3)	730 (2.2)
H-1 → L	470 (0.2)	520 (1.2)
H → L+1	379 (1.0)	395 (3.0)

[a]CAS(6,4) and CAS(6,6) active spaces have been used, respectively. Excitation energies are given in nanometers. Oscillator strengths are given within parentheses (for the experimental values, extinction coefficients, divided by 10^4, are given).

negligible oscillator strengths; the extended results with all transitions are given in SI Table S3). The calculated vertical electronic transitions for the π-$[TCNE]_2^{2-}$ dimer match the absorption bands observed in the UV−vis spectrum (with a relative error lower than 2% in both excitation energies). On the other hand, the predicted vertical electronic transitions for the π-$[TTF]_2^{2+}$ dimer also match the experimental absorption bands, although the agreement is less satisfactory in this case

DOI: 10.1021/acs.jctc.5b00381
J. Chem. Theory Comput. XXXX, XXX, XXX−XXX

(the relative errors are of ∼8% for the two lowest excitation energies). In addition, the predicted oscillation strengths are also given in Table 2, along with the experimental extinction coefficients. Whereas the absorption intensities are properly predicted for π-$[TTF]_2^{2+}$, the relative intensity between the two electronic excitations is not well reproduced for the π-$[TCNE]_2^{2-}$ dimer.

A.2. TD-DFT Vertical Electronic Transitions. In the present section the vertical electronic transitions for both dimers are evaluated by means of TD-DFT calculations and compared to the experimental bands and the previous CASPT2 results. As shown earlier, the lowest electronic excitation energy converges with the basis set size at the TZP contraction for CASPT2 calculations. Similarly, several basis sets have been assessed for TD-DFT excitation energies. Pople's basis set series 6-31+G(d), 6-311G, 6-311G(d), 6-311+G(d), and 6-311+G(2d) was used for obtaining the lowest excitation energy for the π-$[TCNE]_2^{2-}$ dimer, with the PBE0 and ωB97X density functionals (Table 3). For both functionals, diffusion functions must be included to reach quantitative results, and they have even a major impact than increasing from double-ζ to triple-ζ. Additionally, the lowest excitation energy has also been obtained with the TZVP, def2-TZVP, and aug-cc-pVTZ basis sets, providing close values to the more extended Pople basis sets results.

Table 3. Lowest Vertical Electronic Transition for the π-$[TCNE]_2^{2-}$ Dimer Obtained at the ωB97X and PBE0 Levels Using Different Basis Sets, in CH_2Cl_2 Solution Environment (PCM Solvation Model)[a]

basis set	PBE0	ωB97X
6-31+G(d)	565	610
6-311G	558	599
6-311G(d)	556	599
6-311+G(d)	566	613
6-311+G(2d)	568	614
TZVP	564	610
def2-TZVP	565	612
aug-cc-pVTZ	568	616

[a]The calculations were performed at the PBE-D2/6-31+G(d) optimized geometry in PCM-CH_2Cl_2 solution.

The TD-DFT electronic excitation energies were evaluated for 10 density functionals. The PBE, B97-D3(BJ), M06-L, B3LYP, PBE0, M06-2X, M06-HF, ωB97X, LC-ωPBE, and LC-BLYP functionals have been benchmarked to the experimental bands obtained from the UV−vis spectra of the π-$[TCNE]_2^{2-}$ and π-$[TTF]_2^{2+}$ dimers. This set of functionals accounts for a representative group of density functionals, comprising pure GGA and meta-GGA, hybrid GGA and meta-GGA (with 20, 25, 54, and 100% HF exchange), and RSH functionals. Based on the previous results, the 6-311+G(d) basis set was used for all functionals. The solution environment was modeled using the PCM solvation model (dichloromethane and acetone for π−π-$[TCNE]_2^{2-}$ and π-$[TTF]_2^{2+}$, respectively). Table 4 collects the lowest two (π-$[TCNE]_2^{2-}$) and three (π-$[TTF]_2^{2+}$) excitation energies obtained at the TD-DFT level using the aforementioned functionals. For the lowest energy excitation (H → L), pure GGA functionals predict higher energies than RSH functionals, for both dimers. On the other hand, for the H-1 → L and H → L+1 excitations, pure GGA energies are lower compared to those obtained using RSH functionals. In fact, TD-DFT excitation energies correlate with the degree of HF exchange, Figure 3 (the HF exchange content of each RSH functional is estimated as proposed in the literature;[78,79] see SI Figure S3). In particular, the first excitation for both dimers and the third excitation for the π-$[TTF]_2^{2+}$ dimer are best reproduced with pure functionals, whereas the H-1 → L excitation would be best predicted for both dimers with a hybrid functional with ca. 15% HF exchange. The mean absolute error (MAE) for each functional and dimer with respect to the experimental values is given in Figure 4. Pure GGA and meta-GGA functionals and hybrid functionals with a low amount of HF exchange (<25%) perform notably better than density functionals with a high portion of HF exchange, leading to MAEs around 12−27 nm. On the contrary, the latter functionals (>50% HF exchange) can even reach MAEs of 110 nm. These results can be compared to those obtained at the CASPT2 level. Remarkably, the MAE obtained with the latter methodology is substantially lower for the π-$[TCNE]_2^{2-}$, whereas TD-DFT calculations (HF exchange < 25%) provide better results for the π-$[TTF]_2^{2+}$ dimer.

The impact of the dispersion energy on the computed UV−vis spectrum was also analyzed. Common density functionals

Table 4. Vertical Electronic Transitions for the π-$[TCNE]_2^{2-}$ and π-$[TTF]_2^{2+}$ Dimers Obtained with Several DFT Functionals[a]

	π-$[TCNE]_2^{2-}$		π-$[TTF]_2^{2+}$		
	H → L	H-1 → L	H → L	H-1 → L	H → L+1
PBE	550 (0.4)	390 (0.3)	710 (0.3)	530 (0.1)	360 (0.6)
B97-D3(BJ)	556 (0.4)	391 (0.3)	724 (0.3)	538 (0.1)	358 (0.6)
M06-L	555 (0.4)	376 (0.3)	717 (0.3)	507 (0.2)	340 (0.7)
B3LYP	572 (0.4)	368 (0.3)	732 (0.3)	511 (0.2)	341 (0.6)
PBE0	566 (0.4)	360 (0.4)	731 (0.3)	497 (0.2)	335 (0.6)
M06-2X	586 (0.4)	340 (0.4)	788 (0.3)	473 (0.2)	326 (0.6)
M06-HF	577 (0.5)	321 (0.5)	924 (0.4)	457 (0.3)	320 (0.5)
ωB97X	613 (0.4)	339 (0.4)	852 (0.4)	472 (0.2)	316 (0.6)
LC-ωPBE	617 (0.5)	331 (0.5)	883 (0.4)	461 (0.2)	311 (0.6)
LC-BLYP	622 (0.5)	327 (0.5)	893 (0.4)	464 (0.2)	305 (0.6)

[a]Oscillator strength values are given within parentheses. Calculations performed in dichloromethane and acetone solution (modeled using the PCM continuous model), respectively, using the 6-311+G(d) basis set. The calculations were carried out at the PBE-D2/6-31+G(d) optimized geometry in PCM solution. As indicated in Table 2, the lowest energy experimental absorption bands of π-$[TCNE]_2^{2-}$ are centered at 525 and 370 nm, while those of π-$[TTF]_2^{2+}$ are centered at 730, 520, and 395 nm.

DOI: 10.1021/acs.jctc.5b00381
J. Chem. Theory Comput. XXXX, XXX, XXX−XXX

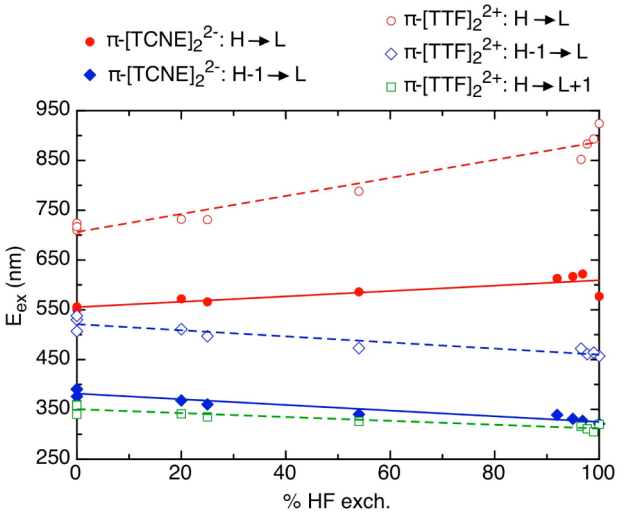

Figure 3. Excitation energies obtained at the TD-DFT level as a function of the HF exchange portion, for the π-$[TCNE]_2^{2-}$ and π-$[TTF]_2^{2+}$ dimers. The 6-311+G(d) basis set was used, and all calculations were performed in the PCM solution.

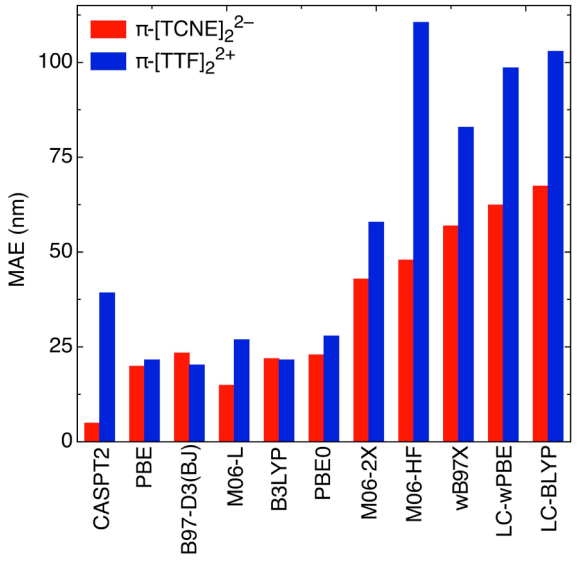

Figure 4. Mean absolute error (MAE) associated with excitation energies (nm) for the TD-DFT and CASPT2 calculations of Table 4 and Table 2, respectively. Values compared to the experimental energies.

usually do not provide a correct description of dispersion, associated with medium- and long-range correlation. A popular approach to account for dispersion is the Grimme correction, which adds an empirical term to the total $E_{KS\text{-}DFT}$ energy. Vertical electronic excitation energies obtained using PBE and PBE-D3(BJ) led to the same exact result. This is not surprising as Grimme's dispersion schemes only depend on atom-pairwise fitted coefficients and not on the converged electron density,[49,80,81] and thus there is no variation from the ground state to the excited states. Alternatively, vertical electronic transitions obtained with density functionals that majorly do not account for dispersion (for instance PBE) were also compared to those that successfully do. The Minnesota set of functionals (e.g., M06-L, M06-2X, and M06-HF),[50,53] are parameterized to account for medium-range correlation and hence perform satisfactorily on dispersion interactions.[82] Despite providing PBE and M06-L similar excitation energies, the small differences by no means can be directly assigned to dispersion. Additionally, M06-2X and M06-HF are also parameterized to account for dispersion, and their performance is notably worse than low HF exchange functionals, including M06-L. Therefore, the amount of exact exchange seems to be a more critical factor than dispersion for the description of vertical excitation energies.

It is worth finally noting that TD-DFT oscillator strengths are in better agreement with the experimental relative intensities than those previously found at the CASPT2 level. Both methods predict the correct intensities for the π-$[TTF]_2^{2+}$ dimer, but whereas CASPT2 predicts for π-$[TCNE]_2^{2-}$ the second excitation to be twice as intense as the lowest excitation, TD-DFT anticipates the latter to be 30% higher than the former excitation. This is in close accordance with the ∼35% relative intensity observed in the experiments.

B. Dynamic Perspective. Thermal fluctuations have been increasingly acknowledged to be a key ingredient when comparing computed spectra with experimental data.[37−46] In the following, these fluctuations have been investigated by performing a 45 ps CPMD simulation of the π-$[TCNE]_2^{2-}$ dimer in a CH_2Cl_2 simulation box at 175 K and evaluating its excitation energies on 100 configurations extracted from the simulation (further details are given in Methodology). Based on the previous results, at each extracted configuration the CH_2Cl_2 molecules are removed for the vertical electronic transitions calculation, and the solution environment was modeled using the PCM method.

The simulation explores C···C distances in the 2.6−3.2 Å range between the $[TCNE]^{\bullet-}$ units and leads to an average long-bond distance of 2.9 Å, in perfect agreement with the experimental value reported for several molecular crystals containing π-$[TCNE]_2^{2-}$ dimers.[83,84] Moreover, the average angle and dihedral angle between the four central carbon atoms directly involved in the bond (as defined in SI Figure S4) results in 90° and almost 0°, respectively, with thermal distributions that span about 10° above and below these mean values. Hence, the π-$[TCNE]_2^{2-}$ dimer do not dissociate, as experimentally observed at this temperature.[14] From this entire trajectory, 100 configurations evenly distributed over the running time were taken for a subsequent evaluation of the excitation energies and oscillator strengths with CASPT2 and TD-DFT methods. These results will provide a dynamic perspective of the absorption spectrum of π-$[TCNE]_2^{2-}$ in solution. The evolution of the structural parameters along the 45 ps simulation and that for the 100 extracted configurations is shown in SI Figure S4, evidencing that the distribution of the configurations considered is well balanced for the three variables. In addition, the mean values obtained in both cases validate the suitability of the sample to quantitatively represent the whole trajectory (SI Table S4). The CAS(6,4) active space was used for the CASPT2 calculations with the TZP contraction of the ANO-L basis set, and the B97-D3(BJ)/6-311+G(d) was used for the TD-DFT analysis, according to the previous section results. Thermal fluctuations may permute the order of two or more excited states. Thus, to ensure that the two characteristic absorption bands were taken into account on each configuration, 5 and 10 singlet electronic states were evaluated for the CASPT2 and TD-DFT calculations, respectively (all other electronic transitions but the two of interest present negligible oscillator strength).

DOI: 10.1021/acs.jctc.5b00381
J. Chem. Theory Comput. XXXX, XXX, XXX−XXX

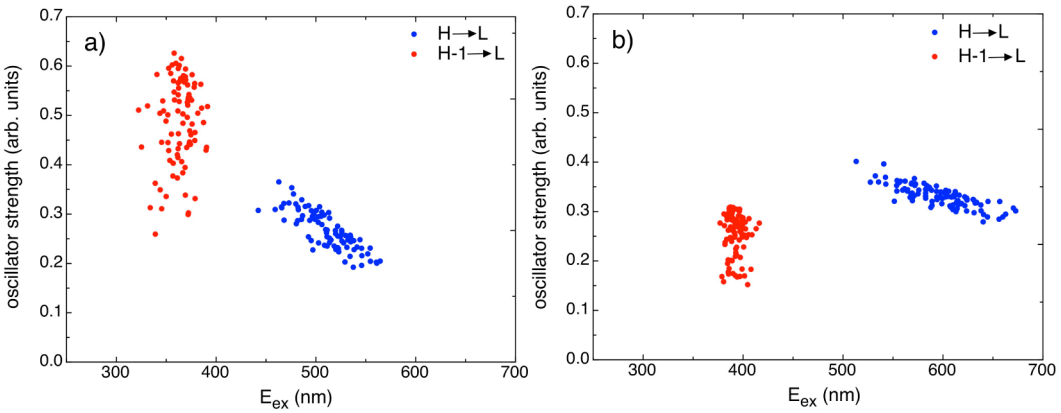

Figure 5. Absorption spectrum of π-$[TCNE]_2^{2-}$ in dichloromethane obtained at (a) CAS(6,4)PT2 and (b) TD-DFT levels. The TZP contraction of the ANO-L basis set was used for CASPT2, and B97-D3(BJ) functional with 6-311+G(d) basis set was used for TD-DFT calculations. The PCM solvation model was used for both methods.

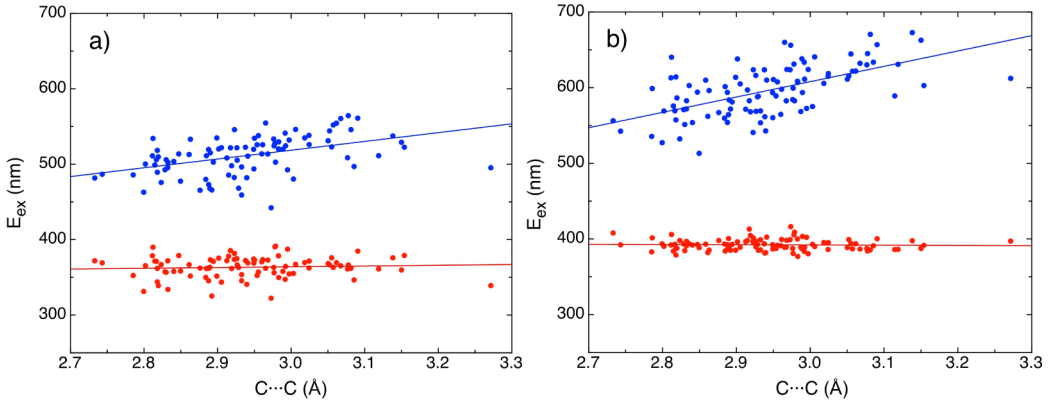

Figure 6. H → L (blue) and H-1 → L (red) excitation energies of the π-$[TCNE]_2^{2-}$ as a function of the intermonomer C···C distance between the $[TCNE]^{\bullet-}$ units, obtained at the (a) CASPT2 and (b) TD-DFT levels on the 100 configurations taken from the AIMD simulation. The TZP contraction of the ANO-L basis set was used for CASPT2, and B97-D3(BJ) functional with 6-311+G(d) basis set was used for TD-DFT calculations. The PCM solvation model was used for both methods.

The absorption spectrum of π-$[TCNE]_2^{2-}$ in dichloromethane obtained using both methods is shown in Figure 5. Thermal fluctuations trigger a negligible shift of the mean values obtained at the CASPT2 level (512 and 363 nm) compared to the previous section static results (516 and 369 nm). On the other hand, a deviation of 40 nm to lower energies is obtained for the H → L transition at the TD-DFT level, leading to an average value of 596 nm (556 nm using the static approach). This results in a larger relative error for the dynamic approach (12%) than the static approach (5%) when compared to the experimental band, 525 nm. Interestingly, thermal dispersion is notably higher on the H → L transition than on the H-1 → L, for both methods, thus manifesting a greater impact of the dynamic effects due to thermal motion on the lowest energy excitation than on the second lowest transition. No significant thermal effects are observed on the relative intensities between the two absorption bands.

The different thermal dispersion presented by the two lowest electronic transitions was investigated by analyzing the dependence of the vertical excitation energies with the geometrical intermonomer parameters (namely, the distance, angle, and dihedral angle) between the $[TCNE]^{\bullet-}$ units, at each conformation extracted from the simulation. Figure 6 shows the variation of the excitation energies with the C···C intermonomer distance, while SI Figure S5 shows their variation with the angle and dihedral angle. The H-1 → L transition is not affected by any structural arrangement caused by the thermal motion. However, the H → L exhibits a rather strong dependence with the intermonomer distance (no correlation is manifested with the angle and dihedral angle). In this monodimensional scenario, the linear trend observed for the first vertical excitation energy explains the resulting ∼150 nm bandwidth. Other geometrical distortions should be evaluated in order to account for all of the oscillations of the excitation energy due to thermal effects, but this is not feasible from a practical point of view.

These larger thermal effects for the H → L transition compared to the negligible effects for the H-1 → L can be rationalized by taking into account the nature of the orbitals involved in each transition. The H → L excitation involves a π-bonding and a π-antibonding molecular orbitals, while the H-1 → L transition occurs between two π-antibonding orbitals (Figure 2a). Bonding orbitals are stabilized at shorter intermonomer distances due to higher SOMO−SOMO overlap, whereas antibonding orbitals follow the opposite trend. Hence, any transition between two π-orbitals of different nature will be affected by the intermonomer stretching normal mode and, on the other hand, transitions between two orbitals of the same nature will essentially remain unaffected. To validate this hypothesis, Figure 7 shows the DFT orbital

DOI: 10.1021/acs.jctc.5b00381
J. Chem. Theory Comput. XXXX, XXX, XXX−XXX

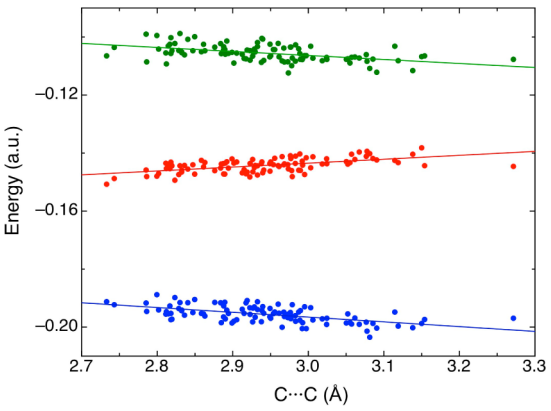

Figure 7. Dependence of the HOMO-1 (blue), HOMO (red), and LUMO (green) orbital energies of π-$[TCNE]_2^{2-}$ with the C···C distance between the monomer units. DFT results for the 100 configurations extracted from the AIMD simulation. Calculations were done at the B97-D3(BJ)/6-311+G(d) level.

energies as a function of the C···C distance. The energy of the HOMO-1 and LUMO orbitals decreases when the intermonomer distance is increased because of their π-antibonding character, while the HOMO orbital is destabilized. Consequently, the H−L gap is affected by the intermonomer distance variation, whereas the H-1 → L transition remains practically constant over the whole range of distances. Interestingly, this analysis allows us to predict a similar behavior for the three lowest transitions of the π-$[TTF]_2^{2+}$ dimer. As shown in the experimental spectrum,[15] the lowest energy excitation (H → L) presents a broader band than the other two transitions (H-1 → L and H → L+1). The HOMO and LUMO+1 are π-bonding orbitals, whereas the HOMO-1 and LUMO orbitals are π-antibonding and, therefore, the H → L transition is more sensitive to the intermonomer stretching mode. Finally, no significant variations are observed for the DFT orbital energies as a function of the angle and dihedral variations (SI Figure S6), consistent with the noneffect of these parameters on the excitation energies.

CONCLUSIONS

The suitability of CASPT2 and TD-DFT methods for the description of vertical electronic excitations in dimers between radical ions presenting long, multicenter bonding has been extensively evaluated throughout this work. The π-$[TCNE]_2^{2-}$ and π-$[TTF]_2^{2+}$ dimers served as the cornerstone to benchmark several active spaces and 10 density functionals, as well as various basis sets. The impact of the thermal motion was also assessed for π-$[TCNE]_2^{2-}$ based on 100 configurations extracted from a molecular dynamics simulation of the dichloromethane solution environment at 175 K.

Our results show that CASPT2 provides excitation energies very close to the experimental absorption bands for the π-$[TCNE]_2^{2-}$ dimer, with a mean absolute error (MAE) of only 5 nm for the two lowest transitions. The MAE increases up to 39 nm for the π-$[TTF]_2^{2+}$, averaging the three lowest excitations. The results obtained with several active spaces were compared with those obtained with the full π-space, i.e., RAS(22,20) and RAS(26,20) for π-$[TCNE]_2^{2-}$ and π-$[TTF]_2^{2+}$, respectively. No improvement on the first excitation energy is found for π-$[TTF]_2^{2+}$ whenever an active space larger than the minimum (2,2) is chosen; e.g., CAS(2,4), and even a CAS(6,6) provided an E_{ex} closer to the experimental band than the more extended RAS(26,20). On the other hand, for π-$[TCNE]_2^{2-}$, RAS(22,20) improves the CAS(6,4) and CAS(4,3) results by 10 nm for the lowest excitation energy.

Interestingly, TD-DFT excitation energies provide better results for π-$[TTF]_2^{2+}$ than CASPT2. Pure GGA and meta-GGA, and hybrid functionals with HF exchange portion lower than 25% reach MAE 15−20 nm lower than CASPT2 excitation energies. Our study reveals that hybrid density functionals with HF exchange > 50% (and, thus, RSH functionals) provide large MAE, higher than 50 nm (even >110 nm for the M06-HF functional). Remarkably, TD-DFT oscillator strengths properly reproduce the absorption bands relative intensities, whereas CASPT2 fails to reproduce the correct order of π-$[TCNE]_2^{2-}$ intensities. Overall, we have shown that cost-efficient methods such as TD-DFT are a reliable tool to predict excitation energies of long-bonded dimers between radical ions.

Finally, the investigation of the thermal fluctuations effects on the UV−vis spectrum of the π-$[TCNE]_2^{2-}$ dimer at 175 K shows that the variation of the energy of the orbitals involved in the lowest energy excitations in response to changes in the intermonomer distance depends on the nature of each orbital (specifically, on whether this orbital is π-bonding or π-antibonding). Therefore, transitions between orbitals of the same nature essentially remain unaffected by the thermal motion, while transitions between orbitals of the opposite nature are sensitive to it. This fact elucidates why the lowest H → L absorption presents a broad band and the following H-1 → L absorption exhibits a narrower band.

ASSOCIATED CONTENT

Supporting Information

Figures showing RAS(22,20) molecular orbitals for the π-$[TCNE]_2^{2-}$ dimer, RAS(26,22) molecular orbitals for the π-$[TTF]_2^{2+}$ dimer, the HOMO−LUMO gap as a function of the % HF exchange, evolution of the distance, the angle, and dihedral angle between $[TCNE]^{\bullet-}$ units, excitation energies as a function of the angle and dihedral angle, and HOMO-1, HOMO, and LUMO orbital energies as a function of the angle and dihedral angle and tables listing vertical electronic transitions obtained for several geometry optimizations at TD-DFT level, vertical electronic transitions obtained for different solvent models at the TD-DFT level, the full list of the lowest energy excited states at the CASPT2 level, average values for the distance, angle, and dihedral angle between the $[TCNE]^{\bullet-}$ units, and optimized Cartesian coordinates of both dimers. The Supporting Information is available free of charge on the ACS Publications website at DOI: 10.1021/acs.jctc.5b00381.

AUTHOR INFORMATION

Corresponding Author

*E-mail: mcapdevila@iciq.es.

Present Address

[†]Institute of Chemical Research of Catalonia (ICIQ), Av. Països Catalans 16, 43007 Tarragona, Spain.

Funding

This work was financially supported by the MINECO of Spain (MAT2011-25972) and Generalitat de Catalunya (2014 SGR 1422). J.R.-A. gratefully acknowledges the Spanish Government for a "Ramón y Cajal" contract. M.F. thanks the University of Barcelona for a Ph.D. grant.

DOI: 10.1021/acs.jctc.5b00381
J. Chem. Theory Comput. XXXX, XXX, XXX−XXX

Notes

The authors declare no competing financial interest.

■ ACKNOWLEDGMENTS

We thank CSUC and BSC for their generous allocation of computer time in their facilities.

■ REFERENCES

(1) Ferraro, J. R.; Williams, J. M. *Introduction to synthetic electrical conductors*; Academic Press: Orlando, FL, USA, 1987; pp 8−80.
(2) Ishiguro, T.; Yamaji, K.; Saito, G. *Organic superconductors*; Springer: New York, 1998; pp 99−156.
(3) Miller, J. S.; Epstein, A. J. *Angew. Chem., Int. Ed.* **1994**, *33*, 385.
(4) Veciana, J. *π-Electron Magnetism—From Molecules to Magnetic Materials*; Springer: Berlin, 2001; pp 33−60.
(5) Kahn, O. *Molecular Magnetism*; Wiley-VCH: New York, 1993; pp 287−332.
(6) Novoa, J. J.; Lafuente, P.; Del Sesto, R. E.; Miller, J. S. *Angew. Chem., Int. Ed.* **2001**, *40*, 2540.
(7) Del Sesto, R. E.; Miller, J. S.; Lafuente, P.; Novoa, J. J. *Chem.−Eur. J.* **2002**, *8*, 4894.
(8) Miller, J. S.; Novoa, J. J. *Acc. Chem. Res.* **2007**, *40*, 189.
(9) Jakowski, J.; Simons, J. *J. Am. Chem. Soc.* **2003**, *125*, 16089.
(10) Jung, Y.; Head-gordon, M. *Phys. Chem. Chem. Phys.* **2004**, *6*, 2008.
(11) Capdevila-Cortada, M.; Miller, J. S.; Novoa, J. J. *Chem.−Eur. J.* **2015**, *21*, 6410.
(12) Garcia-Yoldi, I.; Mota, F.; Novoa, J. J. *J. Comput. Chem.* **2006**, *28*, 326.
(13) Garcia-Yoldi, I.; Miller, J. S.; Novoa, J. J. *J. Phys. Chem. A* **2009**, *113*, 484.
(14) Lü, J.-M.; Rosokha, S. V.; Kochi, J. K. *J. Am. Chem. Soc.* **2003**, *125*, 12161.
(15) Rosokha, S. V.; Kochi, J. K. *J. Am. Chem. Soc.* **2007**, *129*, 828.
(16) Novoa, J. J.; Lafuente, P.; Del Sesto, R. E.; Miller, J. S. *CrystEngComm* **2002**, *4*, 373.
(17) Small, D.; Zaitsev, V.; Jung, Y.; Rosokha, S. V.; Head-Gordon, M.; Kochi, J. K. *J. Am. Chem. Soc.* **2004**, *126*, 13850.
(18) Barin, G.; Coskun, A.; Friedman, D. C.; Olson, M. a; Colvin, M. T.; Carmielli, R.; Dey, S. K.; Bozdemir, O. A.; Wasielewski, M. R.; Stoddart, J. F. *Chem.−Eur. J.* **2011**, *17*, 213.
(19) Wang, C.; Dyar, S. M.; Cao, D.; Fahrenbach, A. C.; Horwitz, N.; Colvin, M. T.; Carmieli, R.; Stern, C. L.; Dey, S. K.; Wasielewski, M. R.; Stoddart, J. F. *J. Am. Chem. Soc.* **2012**, *134*, 19136.
(20) Spruell, J. M.; Coskun, A.; Friedman, D. C.; Forgan, R. S.; Sarjeant, A. A.; Trabolsi, A.; Fahrenbach, A. C.; Barin, G.; Paxton, W. F.; Dey, S. K.; Tkatchouk, E.; Colvin, M. T.; Carmielli, R.; Olson, M. A.; Ben1, D.; Caldwell, S. T.; Rosair, G. M.; Hewage, S. G.; Duclairoir, F.; Seymour, J. L.; Slawin, A. M. Z.; G, W. A., III; Wasielewski, M. R.; Cooke, G.; Stoddart, J. F. *Nat. Chem.* **2010**, *2*, 870.
(21) Casado, J.; Mayorga Burrezo, P.; Ramírez, F. J.; López Navarrete, J. T.; Lapidus, S. H.; Stephens, P. W.; Vo, H.-L.; Miller, J. S.; Mota, F.; Novoa, J. J. *Angew. Chem., Int. Ed.* **2013**, *52*, 6421.
(22) Suzuki, S.; Morita, Y.; Fukui, K.; Sato, K.; Shiomi, D.; Takui, T.; Nakasuji, K. *J. Am. Chem. Soc.* **2006**, *128*, 2530.
(23) Huang, J.; Kertesz, M. *J. Am. Chem. Soc.* **2007**, *129*, 1634.
(24) Capdevila-Cortada, M.; Novoa, J. J.; Bell, J. D.; Moore, C. E.; Rheingold, A. L.; Miller, J. S. *Chem.−Eur. J.* **2011**, *17*, 9326.
(25) Chiang, P.-T.; Chen, N.-C.; Lai, C.-C.; Chiu, S.-H. *Chem.−Eur. J.* **2008**, *14*, 6546.
(26) Coskun, A.; Spruell, J. M.; Barin, G.; Fahrenbach, A. C.; Forgan, R. S.; Colvin, M. T.; Carmieli, R.; Benítez, D.; Tkatchouk, E.; Friedman, D. C.; Sarjeant, A. A.; Wasielewski, M. R.; Iii, W. A. G.; Stoddart, J. F. *J. Am. Chem. Soc.* **2011**, *133*, 4538.
(27) Ziganshina, A. Y.; Ko, Y. H.; Jeon, W. S.; Kim, K. *Chem. Commun. (Cambridge, U. K.)* **2004**, 806.
(28) Capdevila-Cortada, M.; Novoa, J. J. *Chem.−Eur. J.* **2012**, *18*, 5335.
(29) Fumanal, M.; Capdevila-Cortada, M.; Miller, J. S.; Novoa, J. J. *J. Am. Chem. Soc.* **2013**, *135*, 13814.
(30) Capdevila-Cortada, M.; Miller, J. S.; Novoa, J. J. *Chem.−Eur. J.* **2014**, *20*, 7784.
(31) Spruell, J. M. *Pure Appl. Chem.* **2010**, *82*, 2281.
(32) Wang, W.-Y.; Kan, Y.-H.; Wang, L.; Sun, S.-L.; Qiu, Y.-Q. *J. Phys. Chem. C* **2014**, *118*, 28746.
(33) Ferrón, C. C.; Capdevila-Cortada, M.; Balster, R.; Hartl, F.; Niu, W.; He, M.; Novoa, J. J.; López Navarrete, J. T.; Hernández, V.; Ruiz Delgado, M. C. *Chem.−Eur. J.* **2014**, *20*, 10351.
(34) Malavé Osuna, R.; Ruiz Delgado, M. C.; Hernández, V.; López Navarrete, J. T.; Vercelli, B.; Zotti, G.; Novoa, J. J.; Suzuki, Y.; Yamaguchi, S.; Henssler, J. T.; Matzger, A. J. *Chem.−Eur. J.* **2009**, *15*, 12346.
(35) Tateno, M.; Takase, M.; Iyoda, M.; Komatsu, K.; Nishinaga, T. *Chem.−Eur. J.* **2013**, *19*, 5457.
(36) Rizalman, N. S.; Ferrón, C. C.; Niu, W.; Wallace, A. L.; He, M.; Balster, R.; Lampkin, J.; Hernández, V.; López Navarrete, J. T.; Ruiz Delgado, M. C.; Hartl, F. *RSC Adv.* **2013**, *3*, 25644.
(37) Pennanen, T. S.; Vaara, J.; Lantto, P.; Sillanpää, A. J.; Laasonen, K.; Jokisaari, J. *J. Am. Chem. Soc.* **2004**, *126*, 11093.
(38) Della Sala, F.; Rousseau, R.; Görling, A.; Marx, D. *Phys. Rev. Lett.* **2004**, *92*, 183401.
(39) Pavone, M.; Cimino, P.; De Angelis, F.; Barone, V. *J. Am. Chem. Soc.* **2006**, *128*, 4338.
(40) Schreiner, E.; Nair, N. N.; Pollet, R.; Staemmler, V.; Marx, D. *Proc. Natl. Acad. Sci. U. S. A.* **2007**, *104*, 20725.
(41) Přecechtělová, J.; Novák, P.; Munzarová, M. L.; Kaupp, M.; Sklenář, V. *J. Am. Chem. Soc.* **2010**, *132*, 17139.
(42) Domingo, A.; Rodríguez-Fortea, A.; de Graaf, C. *J. Chem. Theory Comput.* **2012**, *8*, 235.
(43) Patrick, C. E.; Giustino, F. *Nat. Commun.* **2013**, *4*, 2006.
(44) Domingo, A.; Sousa, C.; de Graaf, C. *Dalton Trans.* **2014**, *43*, 17838.
(45) Vela, S.; Mota, F.; Deumal, M.; Suizu, R.; Shuku, Y.; Mizuno, A.; Awaga, K.; Shiga, M.; Novoa, J. J.; Ribas-Arino, J. *Nat. Commun.* **2014**, *5*, 4411.
(46) Vela, S.; Deumal, M.; Shiga, M.; Novoa, J. J.; Ribas-Arino, J. *Chem. Sci.* **2015**, *6*, 2371.
(47) Capdevila-Cortada, M.; Ribas-Arino, J.; Novoa, J. J. *J. Chem. Theory Comput.* **2014**, *10*, 650.
(48) Perdew, J. P.; Burke, K.; Ernzerhof, M. *Phys. Rev. Lett.* **1996**, *77*, 3865.
(49) Grimme, S.; Ehrlich, S.; Goerigk, L. *J. Comput. Chem.* **2011**, *32*, 1456.
(50) Zhao, Y.; Truhlar, D. G. *J. Chem. Phys.* **2006**, *125*, 194101.
(51) Becke, A. D. *J. Chem. Phys.* **1993**, *98*, 5648.
(52) Lee, C.; Yang, W.; Parr, R. G. *Phys. Rev. B* **1988**, *37*, 785.
(53) Zhao, Y.; Truhlar, D. G. *Theor. Chem. Acc.* **2007**, *120*, 215.
(54) Zhao, Y.; Truhlar, D. G. *J. Phys. Chem. A* **2006**, *110*, 13126.
(55) Chai, J.-D.; Head-Gordon, M. *J. Chem. Phys.* **2008**, *128*, No. 084106.
(56) Vydrov, O. A.; Scuseria, G. E. *J. Chem. Phys.* **2006**, *125*, No. 234109.
(57) Iikura, H.; Tsuneda, T.; Yanai, T.; Hirao, K. *J. Chem. Phys.* **2001**, *115*, 3540.
(58) Becke, A. D. *J. Chem. Phys.* **1988**, *88*, 1053.
(59) Widmark, P.-O.; Malmqvist, P.; Roos, B. O. *Theor. Chim. Acta* **1990**, *77*, 291.
(60) Widmark, P.-O.; Persson, B. J.; Roos, B. O. *Theor. Chim. Acta* **1991**, *79*, 419.
(61) Ditchfield, R.; Hehre, W. J.; Pople, J. A. *J. Chem. Phys.* **1971**, *54*, 724.
(62) Schäfer, A.; Huber, C.; Ahlrichs, R. *J. Chem. Phys.* **1994**, *100*, 5829.
(63) Weigend, F.; Ahlrichs, R. *Phys. Chem. Chem. Phys.* **2005**, *7*, 3297.
(64) Kendall, R. A.; Dunning, T. H.; Harrison, R. J. *J. Chem. Phys.* **1992**, *96*, 6796.
(65) Miertuš, S.; Scrocco, E.; Tomasi, J. *Chem. Phys.* **1981**, *55*, 117.

DOI: 10.1021/acs.jctc.5b00381
J. Chem. Theory Comput. XXXX, XXX, XXX−XXX

(66) Cancès, E.; Mennucci, B.; Tomasi, J. *J. Chem. Phys.* **1997**, *107*, 3032.
(67) Hutter, J.; et al. *CPMD Program Package*, IBM Corp. 1990−2004 and MPI für Festkörperforschung Stuttgart 1997−2001. See also http://www.cpmd.org. Last accessed March 2015.
(68) Grimme, S. *J. Comput. Chem.* **2006**, *27*, 1787.
(69) Vanderbilt, D. *Phys. Rev. B* **1990**, *41*, 7892.
(70) Nosé, S. *Mol. Phys.* **1984**, *52*, 255.
(71) Hoover, W. *Phys. Rev. A* **1985**, *31*, 1695.
(72) Martyna, G. J.; Klein, M. L.; Tuckerman, M. *J. Chem. Phys.* **1992**, *97*, 2635.
(73) Beebe, N. H. F.; Linderberg, J. *Int. J. Quantum Chem.* **1977**, *12*, 683.
(74) Røeggen, I.; Wisløff-Nilssen, E. *Chem. Phys. Lett.* **1986**, *132*, 154.
(75) Koch, H.; Sánchez de Merás, A.; Pedersen, T. B. *J. Chem. Phys.* **2003**, *118*, 9481.
(76) Frisch, M. J.; Trucks, G. W.; Schlegel, H. B.; Scuseria, G. E.; Robb, M. A.; Cheeseman, J. R.; Scalmani, G.; Barone, V.; Mennucci, B.; Petersson, G. A.; Nakatsuji, H.; Caricato, M.; Li, X.; Hratchian, H. P.; Izmaylov, A. F.; Bloino, J.; Zheng, G.; Sonnenberg, J. L.; Hada, M.; Ehara, M.; Toyota, K.; Fukuda, R.; Hasegawa, J.; Ishida, M.; Nakajima, T.; Honda, Y.; Kitao, O.; Nakai, H.; Vreven, T.; Montgomery, J. A., Jr.; Peralta, J. E.; Ogliaro, F.; Bearpark, M.; Heyd, J. J.; Brothers, E.; Kudin, K. N.; Staroverov, V. N; Kobayashi, R.; Normand, J.; Raghavachari, K.; Rendell, A.; Burant, J. C.; Iyengar, S. S.; Tomasi, J.; Cossi, M.; Rega, N.; Millam, N. J.; Klene, M.; Knox, J. E.; Cross, J. B.; Bakken, V.; Adamo, C.; Jaramillo, J.; Gomperts, R.; Stratmann, R. E.; Yazyev, O.; Austin, A. J.; Cammi, R. .; Pomelli, C.; Ochterski, J. W.; Martin, R. L.; Morokuma, K.; Zakrzewski, V. G.; Voth, G. A.; Salvador, P.; Dannenberg, J. J.; Dapprich, S.; Daniels, A. D.; Farkas, Ö.; Foresman, J. B.; Ortiz, J. V.; Cioslowski, J.; Fox, D. J. *Gaussian09*, Revision D.01; Gaussian: Wallingford, CT, USA, 2009.
(77) Aquilante, F.; De Vico, L.; Ferré, N.; Ghigo, G.; Malmqvist, P.-Å.; Neogrády, P.; Pedersen, T. B.; Pitonák, M.; Reiher, M.; Roos, B. O.; Serrano-Andrés, L.; Urban, M.; Veryazov, V.; Lindh, R. *J. Comput. Chem.* **2010**, *31*, 224.
(78) Sini, G.; Sears, J. S.; Brédas, J.-L. *J. Chem. Theory Comput.* **2011**, *7*, 602.
(79) Sutton, C.; Sears, J. S.; Coropceanu, V.; Brédas, J.-L. *J. Phys. Chem. Lett.* **2013**, *4*, 919.
(80) Grimme, S. *J. Comput. Chem.* **2004**, *25*, 1463.
(81) Grimme, S.; Antony, J.; Ehrlich, S.; Krieg, H. *J. Chem. Phys.* **2010**, *132*, No. 154104.
(82) Goerigk, L.; Kruse, H.; Grimme, S. *ChemPhysChem* **2011**, *12*, 3421.
(83) Del Sesto, R. E.; Sommer, R. D.; Miller, J. S. *CrystEngComm* **2001**, *3*, 222.
(84) Miller, J. S.; O'Hare, D. M.; Chakraborty, A.; Epstein, A. J. *J. Am. Chem. Soc.* **1989**, *111*, 7853.

DOI: 10.1021/acs.jctc.5b00381
J. Chem. Theory Comput. XXXX, XXX, XXX−XXX